


Pulse Width Modulation Methods for Minimizing Commutation Torque Ripples in Low Inductance Brushless DC Motor Drives

Juwon Lee , Student Member, IEEE, Gyu Cheol Lim , Student Member, IEEE, and Jung-Ik Ha , Fellow, IEEE

Abstract—This article proposes pulse width modulation (PWM) methods for low inductance brushless dc (BLDC) motor drives that minimize the commutation torque ripples. An uneven current of noncommutation phase generates the commutation torque ripples. In the low inductance BLDC motor drives, two types of time delays in PWM also induce critical torque ripples. In this article, the analyses of the time delays in PWM and their effects are introduced. Then, two PWM methods are proposed to eliminate the time delays in the commutation region and the conduction region, respectively. The commutation period is controlled to be synchronized to the switching period. In addition, the proposed methods synchronize the switching period to the commutation interrupt. As a result, the proposed methods effectively maintain the minimum commutation period as well as minimize the commutation torque ripples in the low inductance BLDC motor drives. The validity of the proposed methods is demonstrated by the simulation and experimental results in various driving conditions. The results show that the commutation period is remarkably shortened and the commutation torque ripples are reduced by 27.6% in comparison to the conventional method.

Index Terms—Brushless dc (BLDC) motor, commutation torque ripples, low inductance, pulse width modulation (PWM), time delay.

NOMENCLATURE

Superscript *	Reference value.
Subscript OG	Outgoing phase value.
Subscript IC	Incoming phase value.
Subscript NC	Noncommutation phase value.

Manuscript received 17 March 2022; revised 1 June 2022; accepted 22 June 2022. Date of publication 13 July 2022; date of current version 3 January 2023. This work was supported in part by the BK21 FOUR program of the Education and Research Program for Future ICT Pioneers, Seoul National University in 2022, in part by Seoul National University Electric Power Research Institute, and in part by the Korea Medical Device Development Fund grant funded by the Korea government (the Ministry of Science and ICT, the Ministry of Trade, Industry and Energy, the Ministry of Health and Welfare, the Ministry of Food and Drug Safety) under Grant 1711138364 and Grant KMDF_PR_20200901_0175. (Corresponding author: Jung-Ik Ha.)

The authors are with the Department of Electrical and Computer Engineering, Seoul National University, Seoul 08826, South Korea (e-mail: wronskian@snu.ac.kr; gclim@snu.ac.kr; jungikha@snu.ac.kr).

Color versions of one or more figures in this article are available at <https://doi.org/10.1109/TIE.2022.3189104>.

Digital Object Identifier 10.1109/TIE.2022.3189104

V_{dc}	DC link voltage.
v_{no}	Neutral-to-ground voltage.
R_s	Stator resistance.
L_s	Equivalent stator inductance ($L - M$).
e_x	Back EMF of x phase.
S_x	Switching state of x phase.
D_x	Duty ratio of x phase.
T_e	Total output torque.
ω_{rm}	Rotor speed.
f_{sw}	Switching frequency.
t_{ci}	Interval of commutation interrupt.
t_{cm}	Period of commutation region.
t_{cd}	Period of conduction region.
t_{rise}	Rising time of IC phase current.
t_{fall}	Falling time of OG phase current.
t_{CSD}	Duration of commutation start delay.
t_{CED}	Duration of commutation end delay.
N_{cm}	Commutation constant.
N_{cd}	Conduction constant.

I. INTRODUCTION

BRUSHLESS dc (BLDC) motor has been widely used in electric vehicles, robots, and industrial equipment as it has high efficiency, high torque density, and a simple control method [1]. Especially, the attention toward the slotless BLDC motor has continuously been increasing as it has no iron loss, magnetic saturation, or cogging torque [2], [3]. From these advantageous properties, the total output torque is only determined by the magnetic torque, which is a product of the phase current and back electromotive force (EMF). In addition, the slotless BLDC motor is suitable for weight reduction, miniaturization, and mass production at a low cost [4]. Accordingly, it is favorably adopted in the small-sized motor drive systems, such as partial prosthetic hand systems, as shown in Fig. 1. Meanwhile, since the value of stator inductance of the slotless BLDC motor is relatively low, a small control error produces large current ripples, which lead to the torque ripples [2]. As a result, a precise control of the phase current that interacts with the back EMF becomes necessary.

In the BLDC motor drive system, a two-phase control method is commonly used, as the conduction loss is reduced and the control method is simple. The commutation torque ripples are the main issue in the two-phase control method, since it becomes

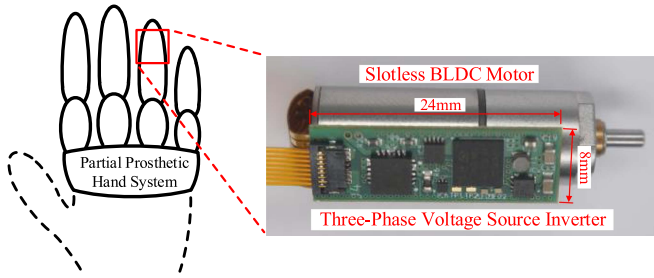


Fig. 1. Partial prosthetic hand system with a slotless BLDC motor and a small-sized three-phase VSI PCB board.

up to 50% of the average torque [5]. Until recently, various pulse width modulation (PWM) methods have been introduced to reduce the commutation torque ripples by keeping constant current of the noncommutation (NC) phase [6]–[14]. The vector selection method considering nonideal back EMF was proposed in [6]. Modified PWM methods using coordinate transformation [7] and PWM-OFF-PWM method [8] were introduced. Also, the methods of changing the current controller using current hysteresis control [9] and integral variable structure control [10] were proposed. However, the previous research neglected the effects of the time delays in PWM, which also generate critical torque ripples in the low inductance BLDC motor drives. In [11], an overlapping control for the slotless BLDC motor was proposed, but the time delay problems still remain. Numerous compensation circuits, such as double-layer C-dump converter [12], diode-assisted buck–boost converter [13], and capacitor-switching-based boost converter [14], were proposed to minimize torque ripples by modulating the dc-link voltage. However, these circuits cannot be applied to a small-sized BLDC motor drive system, since an additional space for power semiconductors, capacitors, and inductors is required.

Meanwhile, the commutation delay is another main factor of the torque ripples. It is generated due to the time delay in PWM and causes various losses in the motor drive system [15], [16]. In the case of BLDC motor drives, the commutating instant does not match with the end of the PWM switching due to the commutation delay [17]. Thus, several methods compensating for the commutation delay were proposed in [18]–[24]. The methods of modifying the carrier function by initializing [18] and changing the frequency [19] at the commutating instant were introduced. However, the PWM duty ratio became an inaccurate value and the current harmonic distortion was generated due to the carrier function, which are critical in the low inductance motor drives. Mixing the ratio of the commutation and conduction period was proposed in [20], but the modified PWM duty ratio was still not precise. To reduce the commutation delay, pulse-amplitude modulation methods using the buck converter [21] and phase-controlled rectifier [22] were proposed. In [23], the PWM generation method using hall signals with the logical circuit was proposed. However, the abovementioned methods required additional circuits that take up considerable space. The commutation error compensation method, which considers both phase delay and position error, was proposed in [24]. Although this method was effective for compensating the position

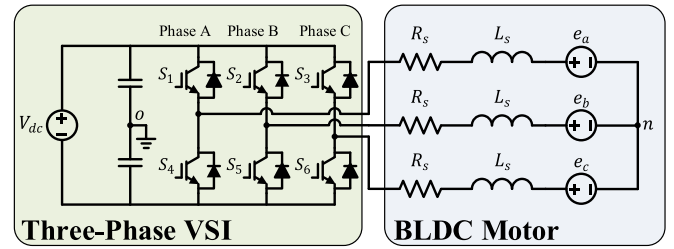


Fig. 2. Equivalent circuit of a BLDC motor with a three-phase VSI.

error, there was still a limit to eliminating the commutation delay.

This article proposes new PWM methods to minimize the commutation torque ripples in the low inductance BLDC motor drives. At first, considering the effect of PWM, the time delays called commutation end delay (CED) and commutation start delay (CSD) are introduced and analyzed. The analyses represent that the torque ripples due to the time delays are critical to the low inductance BLDC motor drives. Then, to eliminate each delay, two types of PWM methods called the N-switching period commutation method and the variable switching period (VSP) conduction method are proposed. The former modifies the PWM duty ratio to synchronize the commutation period to the switching period, and the latter adjusts the switching period to synchronize it to the commutating instant. As a result, the proposed methods effectively remove the time delays and maintain the NC phase current constant. Accordingly, the commutation torque ripples are minimized, and the commutation period is kept to a minimum in the low inductance BLDC motor drives. Finally, the proposed methods are verified by the simulation software, PLECS of Plexim Inc., and experimental results from a partial prosthetic hand system.

II. ANALYSIS OF COMMUTATION TORQUE RIPPLES IN CONVENTIONAL PWM METHOD

A. Modeling of BLDC Motor

Fig. 2 shows the equivalent circuit of the BLDC motor with a three-phase PWM voltage source inverter (VSI). The voltage equations from ground to each phase and ground to the neutral point are expressed as

$$\begin{aligned} v_{ao} &= R_s i_a + L_s \frac{di_a}{dt} + e_a + v_{no} = S_a \frac{V_{dc}}{2} \\ v_{bo} &= R_s i_b + L_s \frac{di_b}{dt} + e_b + v_{no} = S_b \frac{V_{dc}}{2} \\ v_{co} &= R_s i_c + L_s \frac{di_c}{dt} + e_c + v_{no} = S_c \frac{V_{dc}}{2} \\ v_{no} &= \frac{S_a + S_b + S_c}{6} V_{dc} - \frac{e_a + e_b + e_c}{3} \end{aligned} \quad (1)$$

where the switching state S is 1 when the upper switch conducts and -1 when the lower switch conducts. In one switching period t_{sw} , S becomes 1 during the PWM duty ratio Dt_{sw} and -1 in the rest of the time. Using the state-space averaging, the switching state is expressed as $S_{t_{sw}} = 2D - 1$.

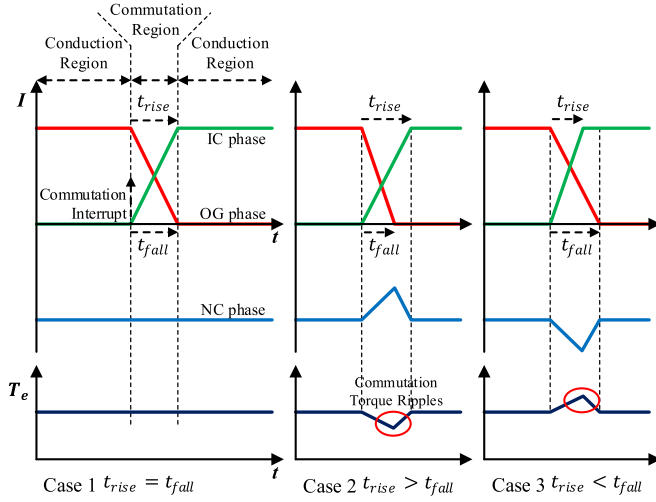


Fig. 3. Various cases of three-phase current waveforms in the two-phase control method of a BLDC motor.

The two-phase control method of the BLDC motor is shown in Fig. 3. The commutation interrupt, which is triggered by the hall sensor or the zero-crossing point of the back EMF, starts at every 60° of the electrical angle. The commutation region occurs when the commutation interrupt is triggered and the conduction region occurs in the rest of the time. In the commutation region, the outgoing (OG) phase current falls to zero and the incoming (IC) phase current rises to the value of the current reference where the NC phase current is determined by the current of the other two phases. Using the Kirchhoff's current law at the neutral point, the total output torque is expressed as

$$\begin{aligned} i_{OG} + i_{IC} + i_{NC} &= 0 \\ T_e &= \frac{e_{OG}i_{OG} + e_{IC}i_{IC} + e_{NC}i_{NC}}{\omega_{rm}} \\ &\approx \frac{E(i_{OG} + i_{IC}) - E i_{NC}}{\omega_{rm}} = -\frac{2E i_{NC}}{\omega_{rm}} \end{aligned} \quad (2)$$

where E is the peak value of trapezoidal back EMF. From (2), the commutation torque ripples are generated when the NC phase current does not remain constant.

Three typical cases of phase current are shown in Fig. 3. In case 1, the rising time of the IC phase current t_{rise} and the falling time of the OG phase current t_{fall} are same, where the NC phase current and the output torque are maintained constant. However, in case 2 or 3, t_{rise} is longer and shorter than t_{fall} , respectively, causing the ripple of NC phase current and output torque. Depending on the motor parameters, the phase current within the commutation region is determined to be one of the abovementioned three cases. Accordingly, the compensation methods are required to achieve the commutation region as case 1.

B. Commutation End Delay

The previous compensation methods only tried to keep t_{rise} and t_{fall} identical. To satisfy the condition, the PWM duty

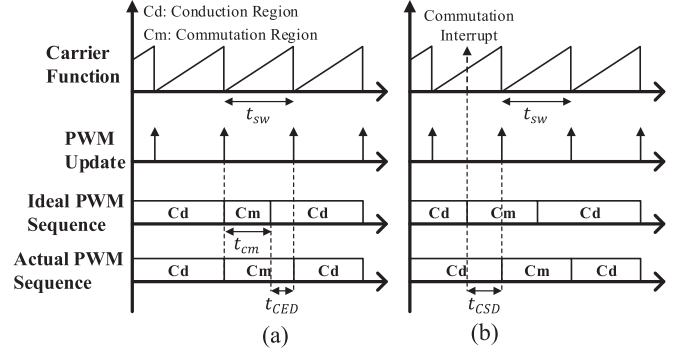


Fig. 4. Ideal and actual PWM sequences of the two-phase control method.

ratio of each phase was calculated. However, in the PWM VSI system, the PWM sequence is updated at every peak of the carrier function, as shown in Fig. 4(a). Therefore, there is a time delay t_{CED} between the end of the commutation region and the next PWM sequence, which is called ‘‘CED’’. The CED has a value between zero and t_{sw} . As the PWM duty ratio stays constant until the next peak of the carrier function, the PWM sequence remains unchanged even if the commutation region ends. As a result, the torque ripples occur during CED even though the compensation method is applied. Assuming constant back EMF during the commutation region, the CED and the torque ripples are expressed as

$$\begin{aligned} t_{CED} &= N_{cm} t_{sw} - t_{cm}, N_{cm} \in \mathbb{N} \\ \tilde{T}_e &= T_e - T_e^* = \frac{\Delta i}{\Delta t} t_{CED} \frac{e_{IC} - e_{NC}}{\omega_{rm}} \approx \frac{v_L t_{CED}}{L_s} \frac{2E}{\omega_{rm}}. \end{aligned} \quad (3)$$

Therefore, the torque ripples due to commutation delay become severe when the CED is long or the stator inductance is low. Assuming v_L is identical as well as the phase voltage, the commutation torque ripples due to CED are much more critical in the low inductance BLDC motor system.

C. Commutation Start Delay

The commutation interrupt indicates the start of the commutation region and is related to the rotor position. As the rotor position and the PWM sequence are irrelevant, the commutation interrupt could be triggered in between the PWM sequence, as shown in Fig. 4(b). Therefore, a time delay t_{CSD} occurs between the commutation interrupt and the next PWM sequence, which is called ‘‘CSD’’. The CSD has a value between zero and t_{sw} . The lagged commutation due to the time delay induces the torque ripples that are proportional to CSD. Moreover, it generates circulating current and reduces efficiency and various losses of the motor drives [24], [25]. These negative effects are even more severe in the low inductance motor drives and high-speed drives.

The effects of CED and CSD are shown in Fig. 5. Due to the time delays, the PWM sequence in the commutation region is distorted, which induces the commutation torque ripples.

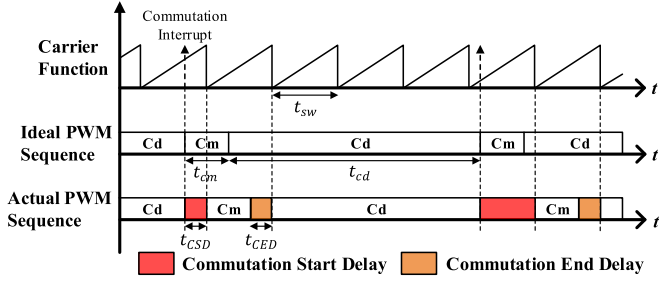


Fig. 5. CSD and CED in ideal and actual PWM sequences.

Meanwhile, it is necessary to minimize the duration of the commutation region to reduce the torque ripples and enhance system response [7], [12]. As the back EMF of OG phase starts decreasing at the commutating instant, the commutation period should be as short as possible to assure constant output torque in the commutation region. In the following section, the novel PWM methods are proposed that minimize the duration of the commutation region as well as eliminate both CED and CSD.

III. PROPOSED PWM METHODS

In order to eliminate the CED and CSD with the minimum commutation period, this article proposes two PWM methods: 1) the N-switching period (NSP) commutation method; and 2) the VSP conduction method.

A. NSP Commutation Method

According to (3), the CED is produced by the time delay between the commutation period and the switching period. The period of commutation region varies in the conventional PWM methods; it depends on the parameters, such as phase current, resistance, and inductance. Therefore, the commutation period and duration of CED become nonperiodical. The prepresented research [26] synchronized the commutation period to a digital sampling period to eliminate CED, but the commutation period was not achieved to be a minimum, since the minimum value becomes shorter than a sampling period when the motor is driven with a higher switching frequency. In the proposed NSP commutation method, the commutation period is synchronized to the multiple of the switching period and N_{cm} , which is called “commutation constant”. Moreover, the commutation period and the commutation constant are controlled to be a minimum.

To control the commutation period, both the rising time of IC phase current and the falling time of OG phase current should be equalized to the multiples of the switching period as follows:

$$t_{cm} = t_{rise} = t_{fall} = N_{cm} t_{sw}, N_{cd} \in \mathbb{N}. \quad (4)$$

As t_{rise} and t_{fall} are determined by the phase voltage and motor parameters, the PWM duty ratio of each phase is modified to satisfy (4). The proposed method is divided into the following two cases according to the relation between the commutation period and the motor electric constant, i.e., $\tau_{elec} = L_s / R_s$.

Short Commutation Period ($t_{cm} < 2\tau_{elec}$): In the case of the short commutation period, the IC phase current rises rapidly to

reach the reference value within a short commutation period. Therefore, the upper switch of the IC phase stays ON and the OG and NC phase switches are controlled, as shown in Fig. 6(a). Thus, the phase voltages and neutral voltage are expressed as

$$\begin{aligned} v_{ICo} &= R_s i_{IC} + L_s \frac{di_{IC}}{dt} + e_{IC} + v_{no} = \frac{V_{dc}}{2} \\ v_{OGO} &= R_s i_{OG} + L_s \frac{di_{OG}}{dt} + e_{OG} + v_{no} = S_{OG} \frac{V_{dc}}{2} \\ v_{NCn} &= R_s i_{NC} + L_s \frac{di_{NC}}{dt} + e_{NC} + v_{no} = S_{NC} \frac{V_{dc}}{2} \\ v_{no} &= \frac{D_{OG} + D_{NC}}{3} V_{dc} - \frac{V_{dc}}{6} - \frac{e_{IC} + e_{OG} + e_{NC}}{3}. \end{aligned} \quad (5)$$

As the IC phase current rises from zero to a reference value and the OG phase current falls from a reference value to zero, each phase current is calculated by solving the differential equations. Using the Taylor's expansion, the phase currents are derived as

$$\begin{aligned} i_{IC} &= \frac{v_{ICn}}{R_s} - \frac{v_{ICn}}{R_s} e^{-\frac{R_s}{L_s} t} \cong \frac{v_{ICn}}{L_s} t \\ i_{OG} &= \frac{v_{OGn}}{R_s} + \left(I^* - \frac{v_{OGn}}{R_s} \right) e^{-\frac{R_s}{L_s} t} \\ &\cong I^* - \frac{R_s I^* - v_{OGn}}{L_s} t \\ i_{NC} &= \frac{v_{NCn}}{R_s} + \left(-I^* - \frac{v_{NCn}}{R_s} \right) e^{-\frac{R_s}{L_s} t} \\ &\cong -I^* + \frac{R_s I^* + v_{NCn}}{L_s} t \end{aligned} \quad (6)$$

$$\begin{aligned} v_{ICn} &= v_{ICo} - e_{IC} - v_{no} \\ &= \frac{(-D_{OG} - D_{NC} + 2) V_{dc} + e_{OG} + e_{NC} - 2e_{IC}}{3} \\ v_{OGn} &= v_{OGO} - e_{OG} - v_{no} \\ &= \frac{(2D_{OG} - D_{NC} - 1) V_{dc} + e_{IC} + e_{NC} - 2e_{OG}}{3} \\ v_{NCn} &= v_{NCn} - e_{NC} - v_{no} \\ &= \frac{(2D_{NC} - D_{OG} - 1) V_{dc} + e_{IC} + e_{OG} - 2e_{NC}}{3}. \end{aligned} \quad (7)$$

To satisfy (4), each phase current should meet

$$\begin{aligned} i_{IC}|_{t=t_{fall}} &= 0 \\ i_{OG}|_{t=t_{rise}} &= I^* \\ i_{NC} &= -I^*. \end{aligned} \quad (8)$$

Using (6)–(8), the rising time of the IC phase current and falling time of the OG phase current are calculated as

$$\begin{aligned} t_{rise} &= \frac{3L_s I^*}{(-D_{OG} - D_{NC} + 2) V_{dc} + e_{OG} + e_{NC} - 2e_{IC}} \\ t_{fall} &= \frac{3L_s I^*}{3R_s I^* - (2D_{OG} - D_{NC} - 1) V_{dc} - e_{IC} - e_{NC} + 2e_{OG}}. \end{aligned} \quad (9)$$

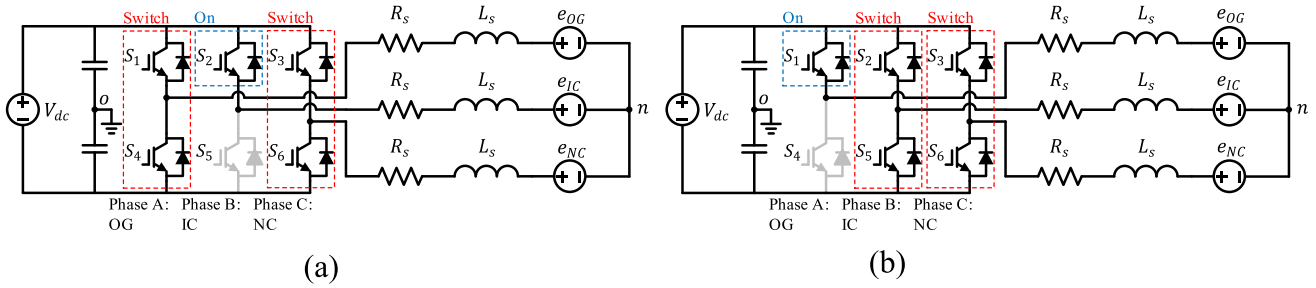


Fig. 6. Switching sequences of the NSP commutation method at the following. (a) Short commutation period. (b) Long commutation period.

And, the PWM duty ratios of OG and NC phases are derived as

$$\begin{aligned} D_{OG} &= \frac{(R_s - 2L_s/t_{cm})I^* + e_{OG} - e_{IC}}{V_{dc}} + 1 \\ D_{NC} &= \frac{(-R_s - L_s/t_{cm})I^* + e_{NC} - e_{IC}}{V_{dc}} + 1. \end{aligned} \quad (10)$$

As the duty ratio exists between 0 and 1, the conditions of the commutation period are expressed as follows:

$$t_{cm} < \frac{2L_s}{R_s} = 2\tau_{elec} \quad (11)$$

$$\begin{aligned} t_{cm} &> \frac{2L_s I^*}{V_{dc} + R_s I^* + e_{OG} - e_{IC}} \cong \frac{2L_s I^*}{V_{dc} + R_s I^*} \\ t_{cm} &> \frac{L_s I^*}{V_{dc} - R_s I^* + e_{NC} - e_{IC}} \cong \frac{L_s I^*}{V_{dc} - R_s I^* - 2E}. \end{aligned} \quad (12)$$

In addition, the period of the commutation region is synchronized to the switching period in the NSP commutation method. Therefore, the minimum values of the commutation constant and the commutation period are expressed as

$$\begin{aligned} N_{cm} &= \left\lceil \max \left\{ \frac{2L_s I^*}{V_{dc} + I^* R_s}, \frac{L_s I^*}{V_{dc} - I^* R_s - 2E} \right\} \times f_{sw} \right\rceil \\ t_{cm} &= N_{cm} t_{sw}. \end{aligned} \quad (13)$$

Using the proposed method, the CED is eliminated, while the commutation period is kept minimized. However, if the switching period is so long that it is not able to satisfy (11) even if $N_{cm} = 1$, another PWM method can be applied.

Long Commutation Period ($t_{cm} > 2\tau_{elec}$): In the case of the long commutation period, the IC phase current rises slowly to reach the reference value within a long commutation period. Therefore, the upper switch of the OG phase stays ON and the IC and NC phase switches are controlled, as shown in Fig. 6(b). Thus, the phase voltages are expressed as

$$\begin{aligned} v_{ICo} &= R_s i_{IC} + L_s \frac{di_{IC}}{dt} + e_{IC} + v_{no} = S_{IC} \frac{V_{dc}}{2} \\ v_{OGo} &= R_s i_{OG} + L_s \frac{di_{OG}}{dt} + e_{OG} + v_{no} = \frac{V_{dc}}{2} \\ v_{NCo} &= R_s i_{NC} + L_s \frac{di_{NC}}{dt} + e_{NC} + v_{no} = S_{NC} \frac{V_{dc}}{2}. \end{aligned} \quad (14)$$

The neutral voltage, phase current, rising time, and falling time are derived in the same way as before. As a result, the

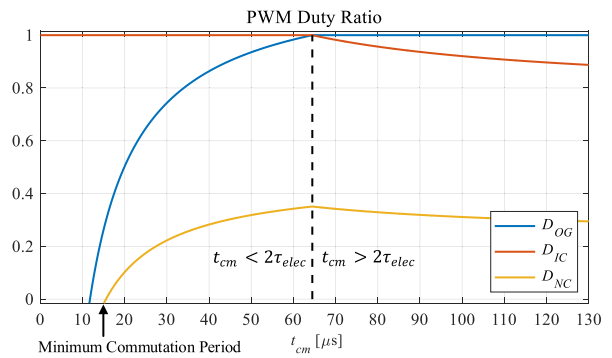


Fig. 7. PWM duty ratio according to the commutation period.

PWM duty ratio of IC and NC phases are expressed as

$$\begin{aligned} D_{IC} &= \frac{(-R_s + 2L_s/t_{cm})I^* + e_{OG} - e_{IC}}{V_{dc}} + 1 \\ D_{NC} &= \frac{(-2R_s + L_s/t_{cm})I^* + e_{NC} - e_{IC}}{V_{dc}} + 1. \end{aligned} \quad (15)$$

And, the condition of the commutation period is derived as

$$t_{cm} > \frac{2L_s}{R_s} = 2\tau_{elec}. \quad (16)$$

In the case of a long commutation period, N_{cm} is always 1, so the commutation period is identical to the switching period.

From (12) and (16), the commutation period is synchronized to the multiples of the switching period in any case of the driving system using the proposed methods. Fig. 7 shows the PWM duty ratio according to the commutation period, where the duty ratio is always between 0 and 1.

In the conventional PWM methods, the commutation period keeps changing while driving. On the other hand, from (10) and (15), the parameters, such as current reference, back EMF, stator resistance, and inductance, are all reflected to calculate the PWM duty ratio. Therefore, the commutation period of the proposed methods is kept constant regardless of the parameters. In addition, the proposed method is implemented using a simple three-phase PWM VSI without any additional circuit.

B. VSP Conduction Method

Fig. 8 shows the carrier function, commutation interrupt, and PWM sequence in the cases of ideal commutation and actual

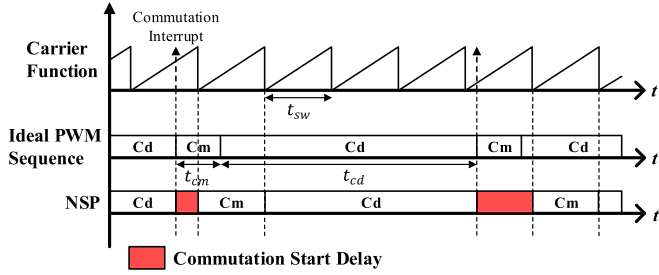


Fig. 8. PWM sequence using the NSP commutation method.

one using the NSP commutation method, respectively. As the timing of the PWM sequence and the commutation interrupt is different, a nonperiodical CSD occurs. To eliminate it, the VSP conduction method is proposed, which is based on the methods usually applied in the six-step control [27]–[29]. The VSP method was used in the case of low-switching frequency modulation, but has not been addressed in the two-phase control of the BLDC motor. In BLDC motor drives, the commutation interrupt occurs at every 60° of the electrical angle. Therefore, the interval of the commutation interrupts t_{ci} is expressed as

$$t_{ci} = t_{cm} + t_{cd} = \frac{3}{\pi\bar{\omega}_r} \quad (17)$$

where $\bar{\omega}_r$ is an average speed between two interrupts, which is calculated using linear extrapolation. To eliminate CSD, the conduction region has to end exactly at the commutating instant. Therefore, the period of conduction region t_{cd} is controlled to be the multiples of the switching period as

$$t_{cd} = N_{cd} t_{sw} = t_{ci} - t_{cm} = \frac{3}{\pi\bar{\omega}_r} - t_{cm}, N_{cd} \in \mathbb{N} \quad (18)$$

where N_{cd} is the conduction constant. In the conventional methods, the commutation period t_{cm} in (18) varies and is complicated to calculate while driving. However, using the proposed NSP commutation method, t_{cm} is fixed and predetermined by the user. Therefore, the conduction period t_{cd} could be controlled by modifying the conduction constant and the switching period. Considering the maximum value of the switching frequency determined by the motor drive system, the conduction constant and the VSP are expressed as

$$N_{cd} = \left\lceil \left(\frac{3}{\pi\bar{\omega}_r} - t_{cm} \right) \times f_{sw_max} \right\rceil$$

$$t'_{sw} = \frac{1}{N_{cd}} \left(\frac{3}{\pi\bar{\omega}_r} - t_{cm} \right). \quad (19)$$

Fig. 9 shows N_{cd} and VSP according to the rotor electric speed. As the speed increase, the conduction constant N_{cd} decreases, and the VSP is calculated using (19). Fig. 10 shows the switching sequence using both the NSP commutation method and the VSP conduction method. Compared to Fig. 8, both CED and CSD are eliminated with minimized commutation torque ripples.

The VSP conduction method is implemented only using a software algorithm without any additional circuit. In addition,

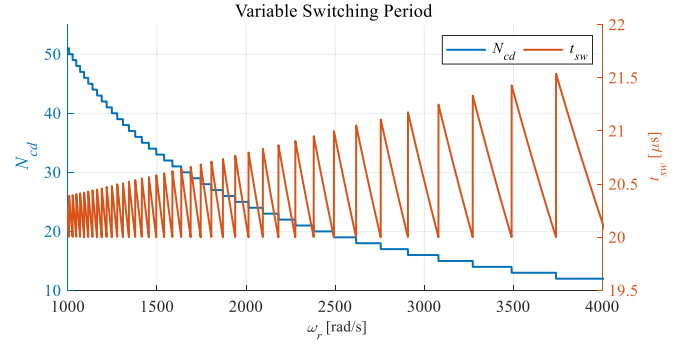


Fig. 9. VSP according to the rotor speed.

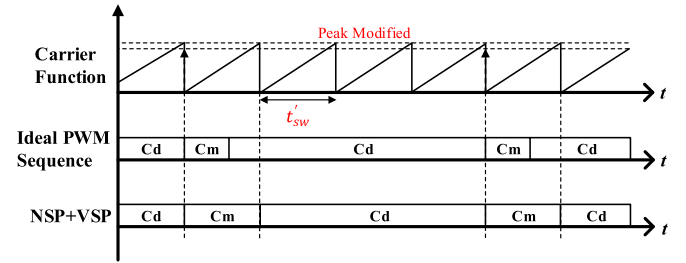


Fig. 10. Modified carrier function and PWM sequence using both the NSP commutation and VSP conduction methods simultaneously.

TABLE I
Parameters of BLDC Motor

Symbol	Parameter	Nominal value
PP	Pole pair	1
V_{dc}	DC link voltage	12 V
I_{rated}	Rated current	0.84 A
T_{rated}	Rated torque	1.62 mNm
R_s	Stator resistance	3.35 Ω
L_s	Stator inductance	108 μH
τ_{elec}	Electric constant	32.28 $\mu\text{H}/\Omega$

the PWM duty ratio is not distorted as the conduction region ends exactly at the commutating instant. As a result, both the time delay and the torque ripples are minimized at the transition from the conduction region to the commutation region.

IV. SIMULATION RESULTS

To verify the proposed PWM methods, the simulation is performed using PLECS. The parameters in Table I are used for the BLDC motor model. Also, the digital signal processor (DSP), the carrier function generator, and the three-phase PWM VSI are implemented.

The three-phase current waveforms using the conventional PWM method, the previous method in [11], and the proposed NSP commutation method are shown in Fig. 11(a). The switching period is modified to ignore the effect of CSD. The torque errors in the figure are expressed as

$$\tilde{T}_e [\%] = \left(\frac{T_{e_max} - T_{e_min}}{T_e^*} \right) \times 100. \quad (20)$$

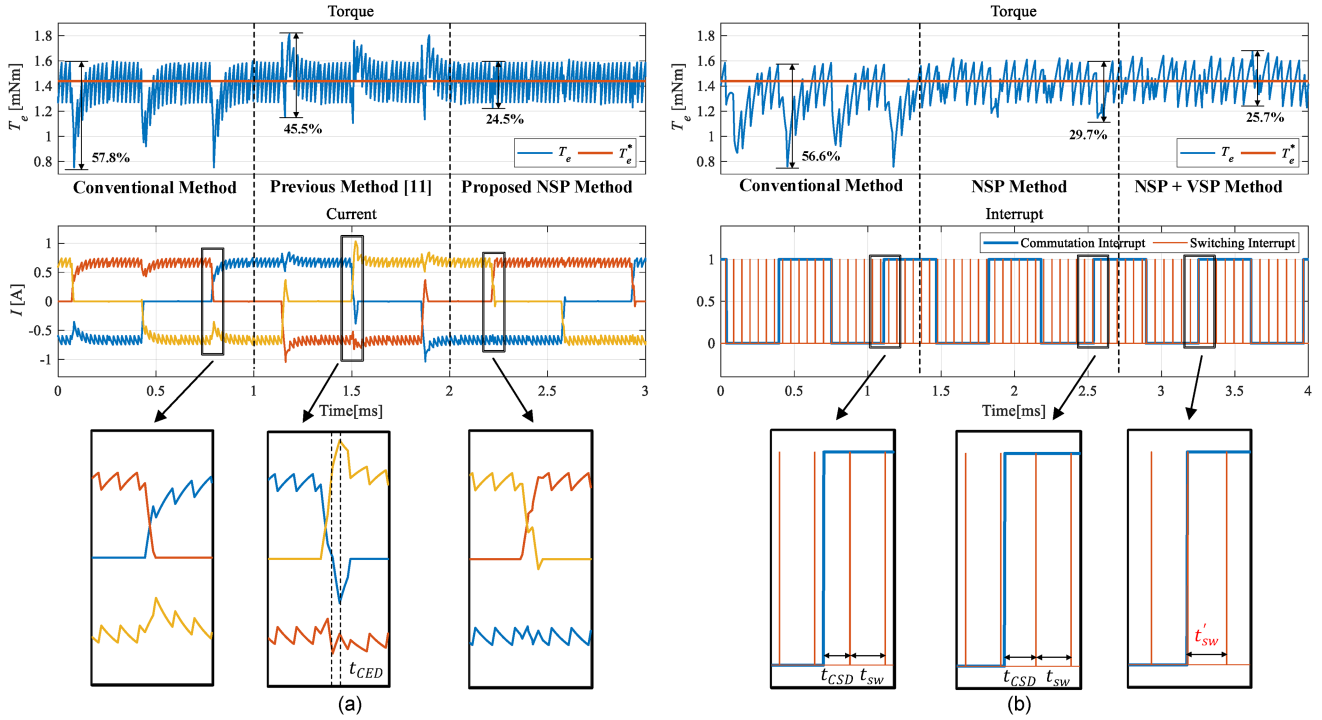


Fig. 11. Simulation results of three-phase current using conventional, previous [11], and proposed NSP and VSP methods at the following. (a) $\omega_{rm} = 30$ kr/min, $f_{sw} = 50$ kHz, and $T_e^* = 0.9T_{rated}$. (b) $\omega_{rm} = 30$ kr/min, $f_{sw} = 18$ kHz, and $T_e^* = 0.9T_{rated}$.

In the conventional method, the falling time is much shorter than the rising time, where the fluctuation of the NC phase current is generated. As addressed in (2), the ripple of the NC phase current induces the commutation torque ripples, which are more than half of the torque reference. In the previous method, in [11], the rising and falling times are equalized as shown in the second waveform of Fig. 11(a). However, there is still CED between the end of the commutation region and the next PWM sequence. Therefore, the commutation torque ripples around half of the torque reference remains even though the compensation method is applied. On the other hand, the torque ripples are minimized in the proposed NSP commutation method. In the last waveform of Fig. 11(a), both the rising and falling times are synchronized to the switching period. Using (13), the commutation constant N_{cm} is derived as 1 and the commutation period t_{cm} is synchronized to a switching period. Since $2\tau_{elec} = 64.55 \mu\text{H}/\Omega$ from Table I, the criterion of (11) is satisfied showing the validity of the analysis and the proposed methods. As a result, the current of the NC phase is maintained constant and the commutation torque ripples are reduced to 24.5% of the torque reference.

The phase current waveforms using the conventional PWM method, the NSP commutation method only, and the NSP commutation method and VSP conduction method simultaneously are shown in Fig. 11(b). In the conventional method, the CSD and CED exist and the rising and falling times are not equalized, resulting in large torque ripples. Using the NSP commutation method only, the CED is eliminated, while the CSD still remains, as shown in Fig. 11(b). Therefore, the torque ripples still exist, which are proportional to the CSD. Using the NSP commutation

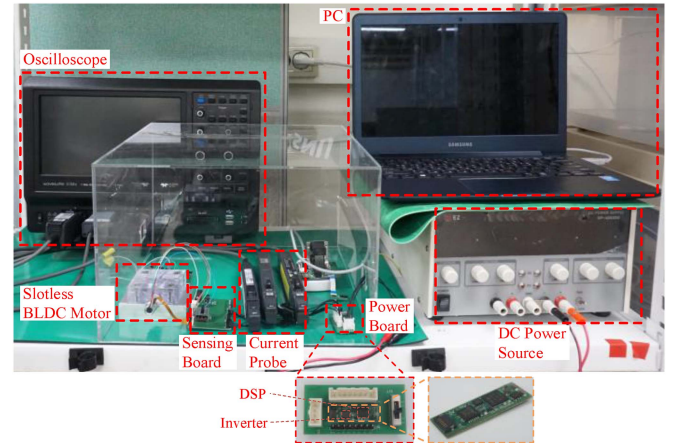


Fig. 12. Experimental setup. The slotless BLDC motor is controlled by small-sized PWM VSI in power PCB board.

method and the VSP conduction method simultaneously, both CSD and CED are eliminated. In the last waveform of Fig. 11(b), the switching period is changed to t'_{sw} , which is synchronized to the commutation interrupt. Using (19), N_{cd} is calculated as 4 and t'_{sw} is calculated as $65.135 \mu\text{s}$. As a result, the torque ripples are reduced to a quarter of the reference torque.

V. EXPERIMENTAL RESULTS

To verify the proposed PWM methods, an experimental setup is established, as shown in Fig. 12. The 10-mm diameter slotless BLDC motor is controlled by the small-sized VSI for the

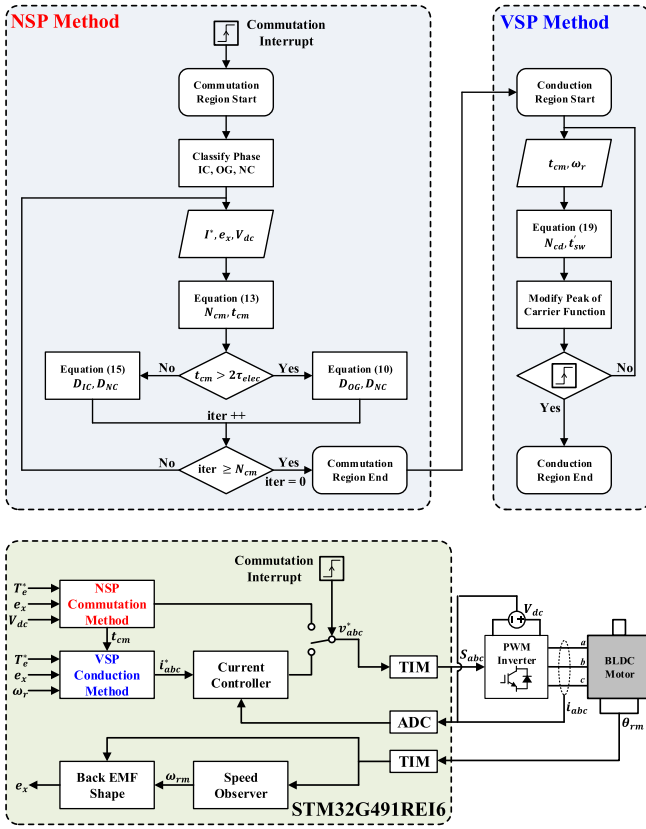


Fig. 13. Block diagram and flowchart of proposed PWM methods.

partial prosthetic hand system. The 5-mm width small DSP (STM32G491RE16) is utilized to implement the proposed methods. Considering the dc-link voltage and the output capacitance of the power semiconductor, the maximum switching frequency of the system is derived as 120 kHz. The parameters of the slotless BLDC motor are listed in Table I.

The overall block diagram and flowchart of the proposed methods are shown in Fig. 13. The phase current and dc-link voltage are sampled by the analog-to-digital conversion (ADC) peripheral, and the rotor position is sampled by timer (TIM) peripheral in the DSP. The rotor position is used to calculate rotor speed by the Luenberger speed observer and reconstruct back EMF. Using the sampled parameters and the torque reference, the NSP commutation method and VSP conduction method are applied in each region, respectively. The switching between two regions is decided by the commutation interrupt and an algorithm in the NSP method. Then, the voltage reference and the PWM duty ratio are derived using the proposed methods and generated by the advanced control timer peripheral in the DSP. In addition, the VSP is implemented by modifying the register related to the peak of the carrier function.

Fig. 14 shows the three-phase currents in the four cases of driving conditions. In Fig. 14(a), the conventional method is applied where the rising and falling times are different and the time delays in PWM exist. Accordingly, the current of the NC phase becomes uneven. In Fig. 14(b), both the NSP commutation method and the VSP conduction method are applied. Using

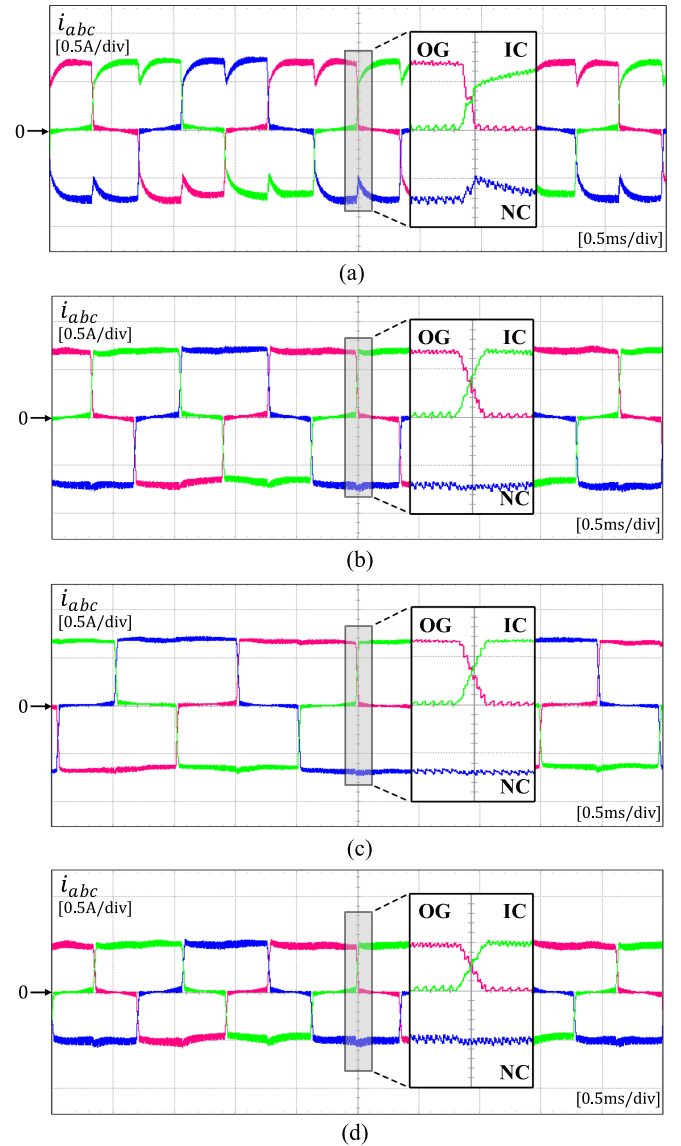


Fig. 14. Experimental results of three-phase current using the following. (a) Conventional method at $\omega_{rm} = 28$ kr/min and $T_e^* = 0.9T_{rated}$. (b) Proposed NSP and VSP methods at $\omega_{rm} = 28$ kr/min and $T_e^* = 0.9T_{rated}$. (c) $\omega_{rm} = 20$ kr/min and $T_e^* = 0.9T_{rated}$. (d) $\omega_{rm} = 28$ kr/min and $T_e^* = 0.6T_{rated}$.

(11), (12), and the parameters in Table I, the conditions of the commutation period are derived as

$$17.75 \mu\text{s} < t_{cm} < 64.55 \mu\text{s}. \quad (21)$$

Therefore, the commutation constant is calculated as 3 and the commutation period is calculated as $25 \mu\text{s}$. In addition, using (19), the VSP t'_{sw} is changed to $8.351 \mu\text{s}$. As a result, both CSD and CED are eliminated and the commutation period is synchronized to three times of the switching period. Therefore, there is no fluctuation in NC phase current. The different speed condition is shown in Fig. 14(c), and the different torque condition is shown in Fig. 14(d). The t_{cm} and t'_{sw} are calculated in the same way. The ripple of the NC phase current is minimized, and the slopes of the OG and IC phase current are identical in

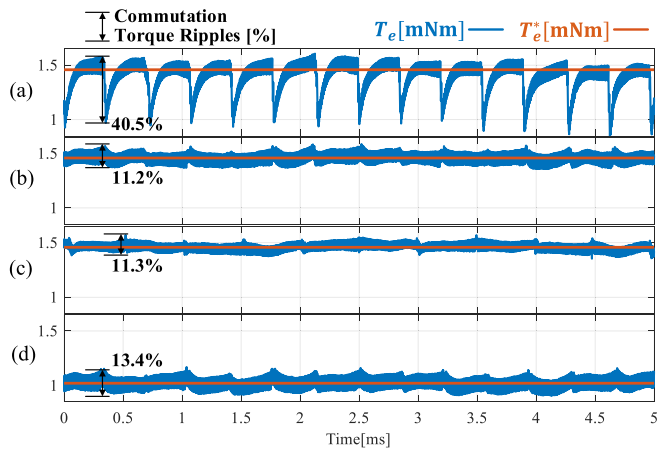


Fig. 15. Waveforms of output torque and torque reference at conditions (a)–(d) in Fig. 14. The commutation torque ripples are calculated at each commutation region.

all three cases of the proposed methods. This demonstrates the validity of the proposed methods even if the control parameters, such as the rotor speed and output torque, are changed.

In Fig. 15, the waveforms of the output torque at condition in Fig. 14(a)–(d) are compared and analyzed. While there are commutation torque ripples of 40.5% using the conventional method, the proposed method reduced the commutation torque ripples to 11.2%, which is 27.6% of the conventional ones. The torque ripples are also minimized in the case of different speed and output torque. Since the remaining torque ripples are generated due to the switching ripples of the phase current, it is considered that the commutation torque ripples are minimized in given driving conditions.

Fig. 16 shows the dynamic response of the proposed methods in varying torque conditions. The proposed NSP commutation method and VSP conduction method are applied in each region. The torque reference is changed from $0.6T_{rated}$ to $0.9T_{rated}$, while the speed is controlled steady to 28 kr/min. It is observed that there are not any current and torque ripples in the transient condition. Moreover, the commutation torque ripples are minimized in both dynamic and steady-state conditions. As a result, the dynamic output torque with fast response and fewer ripples can be obtained using the proposed methods.

The dynamic response of the proposed methods in varying speed conditions is shown in Fig. 17. The speed reference is changed from 14 to 28 kr/min, while the output torque is controlled steady to $0.6T_{rated}$. It is observed that there are not any current and torque ripples in the transient condition even if the speed accelerates in a short period. The output torque is increased in the transient condition, and the commutation torque ripples are effectively minimized in both dynamic and steady-state conditions. This indicates that the proposed methods are also effective in varying speed conditions. As a result, the proposed NSP commutation method and VSP conduction method have both good dynamic and steady-state performance.

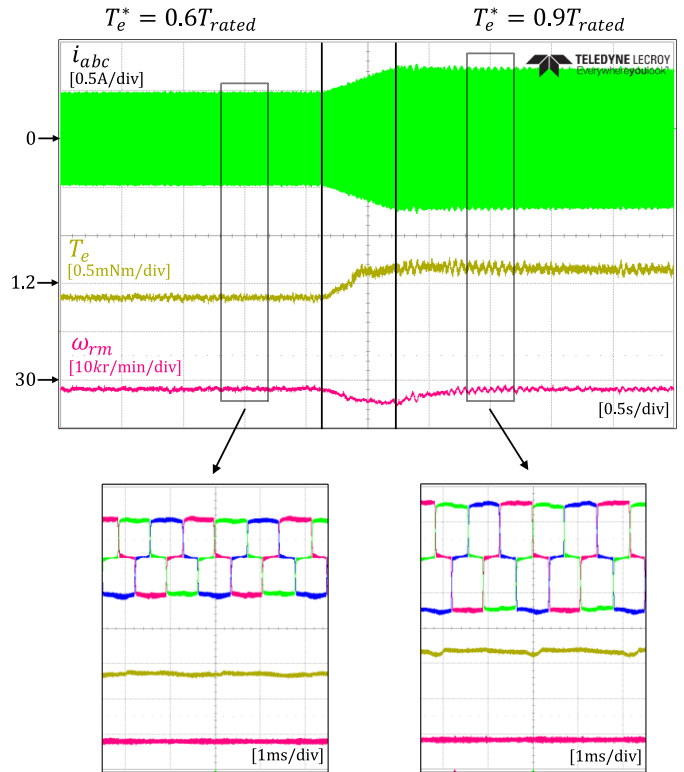


Fig. 16. Experimental results of three-phase current, output torque, and speed in varying torque conditions. The torque reference is changed from $0.6T_{rated}$ to $0.9T_{rated}$.

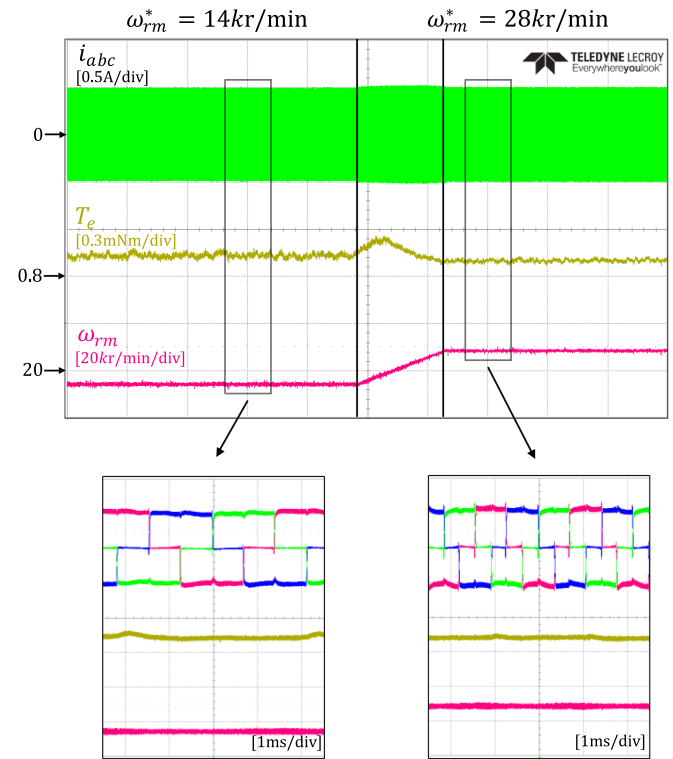


Fig. 17. Experimental results of three-phase current, output torque, and speed in varying speed conditions. The speed reference is changed from 14 to 28 kr/min.

VI. CONCLUSION

This article proposed the PWM methods for minimizing the commutation torque ripples in the low inductance BLDC motor drives. The analyses of CED and CSD represented that the time delays generate critical torque ripples. To eliminate CED, the NSP commutation method was proposed where the commutation period was controlled to be synchronized to the switching period. Then, to eliminate CSD, the VSP conduction method was proposed where the switching period was synchronized to the commutation interrupt. Consequently, both the commutation torque ripples and commutation period were minimized in the low inductance BLDC motor drives. Only a software algorithm and three-phase PWM VSI were required to implement the methods. The proposed methods were verified by the simulation and experimental results in both steady-state and dynamic driving conditions. The results showed that the commutation torque ripples were reduced by 27.6% in comparison to the conventional method. At the same time, the commutation period was minimized and synchronized to three times of the switching period. As a result, the proposed PWM methods provided the high efficiency and precise torque control in various slotless BLDC motor driving applications, such as partial prosthetic hand systems.

REFERENCES

- [1] A. Khazaee, H. A. Zarchi, G. A. Markadeh, and H. M. Hesar, "MTPA strategy for direct torque control of brushless DC motor drive," *IEEE Trans. Ind. Electron.*, vol. 68, no. 8, pp. 6692–6700, Aug. 2021.
- [2] L. Yang, J. Zhao, X. Liu, A. Haddad, J. Liang, and H. Hu, "Effects of manufacturing imperfections on the circulating current in ironless brushless DC motors," *IEEE Trans. Ind. Electron.*, vol. 66, no. 1, pp. 338–348, Jan. 2019.
- [3] G. Burmand, A. Thabuis, D. M. Araujo, and Y. Perriard, "Novel optimized shape and topology for slotless windings in BLDC machines," *IEEE Trans. Ind. Appl.*, vol. 56, no. 2, pp. 1275–1283, Mar./Apr. 2020.
- [4] B. Dehez, F. Baudart, M. Markovic, and Y. Perriard, "Theoretical and experimental investigation of flex-PCB air-gap windings in slotless BLDC machines," *IEEE Trans. Ind. Appl.*, vol. 50, no. 5, pp. 3153–3160, Sep./Oct. 2014.
- [5] R. Carlson, M. Lajoie-Mazenc, and J. C. D. S. Fagundes, "Analysis of torque ripple due to phase commutation in brushless DC machines," *IEEE Trans. Ind. Appl.*, vol. 28, no. 3, pp. 632–638, May/June 1992.
- [6] T. Shi, Y. Cao, G. Jiang, X. Li, and C. Xia, "A torque control strategy for torque ripple reduction of brushless DC motor with nonideal back electromotive force," *IEEE Trans. Ind. Electron.*, vol. 64, no. 6, pp. 4423–4433, Jun. 2017.
- [7] W. Jiang, Y. Liao, J. Wang, P. Wang, and Y. Xie, "Improved control of BLDCM considering commutation torque ripple and commutation time in full speed range," *IEEE Trans. Power Electron.*, vol. 33, no. 5, pp. 4249–4260, May 2018.
- [8] Q. Zhou, J. Shu, Z. Cai, Q. Liu, and G. Du, "Improved PWM-OFF-PWM to reduce commutation torque ripple of brushless DC motor under braking conditions," *IEEE Access*, vol. 8, pp. 204020–204030, 2020.
- [9] W. Jiang, P. Wang, Y. Ni, J. Wang, L. Wang, and Y. Liao, "Multimode current hysteresis control for brushless DC motor in motor and generator state with commutation torque ripple reduction," *IEEE Trans. Ind. Electron.*, vol. 65, no. 4, pp. 2975–2985, Apr. 2018.
- [10] C. Xia, Y. Xiao, W. Chen, and T. Shi, "Torque ripple reduction in brushless DC drives based on reference current optimization using integral variable structure control," *IEEE Trans. Ind. Electron.*, vol. 61, no. 2, pp. 738–752, Feb. 2014.
- [11] J. Fang, X. Zhou, and G. Liu, "Precise accelerated torque control for small inductance brushless DC motor," *IEEE Trans. Power Electron.*, vol. 28, no. 3, pp. 1400–1412, Mar. 2013.
- [12] Y. Xu, Y. Wei, B. Wang, and J. Zou, "A novel inverter topology for brushless DC motor drive to shorten commutation time," *IEEE Trans. Ind. Electron.*, vol. 63, no. 2, pp. 796–807, Feb. 2016.
- [13] Y. Cao, T. Shi, X. Li, W. Chen, and C. Xia, "A commutation torque ripple suppression strategy for brushless DC motor based on diode-assisted buck–boost inverter," *IEEE Trans. Power Electron.*, vol. 34, no. 6, pp. 5594–5605, Jun. 2019.
- [14] R. K. Achary, S. Durgaprasanth, C. Nagamani, and G. S. Ilango, "A simple voltage modulator scheme for torque ripple minimization in a permanent magnet brushless DC motor," *IEEE Trans. Power Electron.*, vol. 35, no. 3, pp. 2809–2818, Mar. 2020.
- [15] H. Zhang et al., "A time-delay compensation method for IPMSM hybrid sensorless drives in rail transit applications," *IEEE Trans. Ind. Electron.*, vol. 66, no. 9, pp. 6715–6726, Sep. 2019.
- [16] C. Choi and W. Lee, "Analysis and compensation of time delay effects in hardware-in-the-loop simulation for automotive PMSM drive system," *IEEE Trans. Ind. Electron.*, vol. 59, no. 9, pp. 3403–3410, Sep. 2012.
- [17] K.-H. Kim and M.-J. Youn, "Performance comparison of PWM inverter and variable DC link inverter schemes for high-speed sensorless control of BLDC motor," *Electron. Lett.*, vol. 38, no. 21, pp. 1294–1295, 2002.
- [18] L. Yang, Z. Q. Zhu, L. Gong, and H. Bin, "PWM switching delay correction method for high-speed brushless DC drives," *IEEE Access*, vol. 9, pp. 81717–81727, 2021.
- [19] D.-K. Kim, K.-W. Lee, and B.-I. Kwon, "Commutation torque ripple reduction in a position sensorless brushless DC motor drive," *IEEE Trans. Power Electron.*, vol. 21, no. 6, pp. 1762–1768, Nov. 2006.
- [20] T. Türker and I. O. K. Khudhair, "A switched current controller with commutation delay compensation for the reduction of commutation torque ripple in BLDCM drives," *Turkish J. Elect. Eng. Comput. Sci.*, vol. 25, no. 4, pp. 2635–2646, 2017.
- [21] C.-L. Huang, C.-J. Wu, and S.-C. Yang, "Full-region sensorless BLDC drive for permanent magnet motor using pulse amplitude modulation with DC current sensing," *IEEE Trans. Ind. Electron.*, vol. 68, no. 11, pp. 11234–11244, Nov. 2021.
- [22] C. Cui, G. Liu, and K. Wang, "A novel drive method for high-speed brushless DC motor operating in a wide range," *IEEE Trans. Power Electron.*, vol. 30, no. 9, pp. 4998–5008, Sep. 2015.
- [23] L. Wang, Z. Zhu, H. Bin, and L. Gong, "A commutation optimization strategy for high speed brushless DC drives with inaccurate rotor position signals," in *Proc. 16th Int. Conf. Ecological Veh. Renewable Energies*, 2021, pp. 1–9.
- [24] L. Wang, Z. Q. Zhu, H. Bin, and L. Gong, "A commutation error compensation strategy for high-speed brushless DC drive based on adaline filter," *IEEE Trans. Ind. Electron.*, vol. 68, no. 5, pp. 3728–3738, May 2021.
- [25] L. Mingyao, L. Qiang, and G. Weigang, "Effect of rotor position error on commutation in sensorless BLDC motor drives," in *Proc. Int. Conf. Elect. Mach. Syst.*, 2005, pp. 497–499.
- [26] J. Lee, G. C. Lim, and J.-I. Ha, "One-digital-sampling commutation method for low inductance brushless DC motor," in *Proc. IEEE Appl. Power Electron. Conf. Expo.*, 2022, pp. 1–7.
- [27] J. Park, S. Jung, and J.-I. Ha, "Variable time step control for six-step operation in surface-mounted permanent magnet machine drives," *IEEE Trans. Power Electron.*, vol. 33, no. 2, pp. 1501–1513, Feb. 2018, doi: [10.1109/tpe.2017.2676703](https://doi.org/10.1109/tpe.2017.2676703).
- [28] H. Yang, Y. Zhang, G. Yuan, P. D. Walker, and N. Zhang, "Hybrid synchronized PWM schemes for closed-loop current control of high-power motor drives," *IEEE Trans. Ind. Electron.*, vol. 64, no. 9, pp. 6920–6929, Sep. 2017.
- [29] H.-G. Choi and J.-I. Ha, "Dynamic current control using synchronous pulse-width modulation for permanent magnet machines," *J. Power Electron.*, vol. 20, no. 2, pp. 501–510, 2020, doi: [10.1007/s43236-020-00038-2](https://doi.org/10.1007/s43236-020-00038-2).



Juwon Lee (Student Member, IEEE) was born in Seoul, South Korea, in 1997. He received the B.S. degree in 2020 from Seoul National University, Seoul, South Korea, where he is currently working toward the Ph.D. degree, all in electrical engineering.

His research interests include electric energy conversions, electric machine drives, and design and control of medical device systems.



Gyu Cheol Lim (Student Member, IEEE) was born in Daejeon, South Korea, in 1993. He received the B.S. degrees from the Georgia Institute of Technology, Atlanta, GA, USA, and the Korea Advanced Institute of Science and Technology, Daejeon, South Korea, in 2016 and 2017, respectively, and the M.S. degree from Seoul National University, Seoul, South Korea, in 2019, all in electrical engineering.

From 2019 to 2020, he was a Research Associate with the Agency for Defense Development, Daejeon, South Korea. Since 2020, he has been a Research Associate with Seoul National University Electric Power Research Institute, Seoul, South Korea. His research interests include high-frequency power converters, electric machines, and their control systems.



Jung-Ik Ha (Fellow, IEEE) was born in South Korea, in 1971. He received the B.S., M.S., and Ph.D. degrees in electrical engineering from Seoul National University, Seoul, South Korea, in 1995, 1997, and 2001, respectively.

From 2001 to 2002, he was a Researcher with Yaskawa Electric Co., Japan. From 2003 to 2008, he was a Senior and Principal Engineer with Samsung Electronics Company, South Korea. From 2009 to 2010, he was a Chief Technology Officer with LS Mecapion Company, South Korea. Since 2010, he has been with the Department of Electrical and Computer Engineering, Seoul National University, where he is currently a Professor. He is also with Electric Power Institute, Seoul National University. From 2016 to 2017, he was a Visiting Scholar with the Massachusetts Institute of Technology, MA, USA. He has authored more than 150 papers, which are published in international journals and conference proceedings in the area of power electronics and motor drives. His research interests include circuits and control in high efficiency and integrated electric energy conversions for various industrial fields.